Identification of wave drift force QTFs for the INO WINDMOOR floating wind turbine based on model test data and comparison with potential flow predictions

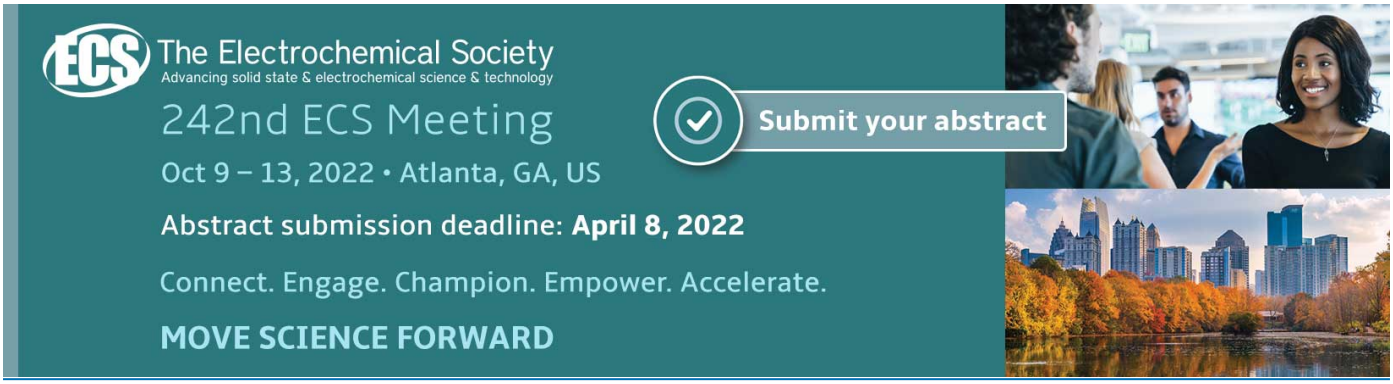

Identification of wave drift force QTFs for the INO WINDMOOR floating wind turbine based on model test data and comparison with potential flow predictions

Nuno Fonseca, Maxime Thys and Petter Andreas Berthelsen

SINTEF Ocean, Marinteknisk senter, Tyholt Otto Nielsens vei 10
7052 Trondheim, Norway

nuno.fonseca@sintef.no

Abstract. The paper presents a comparison between empirical and numerical quadratic transfer functions (QTFs) of the horizontal wave drift loads on the INO WINDMOOR floating wind turbine. The empirical QTFs are determined from cross bi-spectral analysis of model test data obtained in an ocean basin. Validation of the identified QTF is provided by comparing low frequency motions reconstructed from the empirical QTF with measurements. The numerical QTFs are calculated by a panel code that solves the wave-structure potential flow problem up to the second order. Systematic comparisons between numerical and empirical QTFs allows identification of tendencies of empirical QTFs and limitations of the second order potential flow predictions. The study is limited to hydrodynamic loads from waves only, i.e. without current. For small seastates, the results indicate that the second order potential flow predictions of the surge QTFs agree quite well with the wave drift coefficients identified empirically from the model test data. For moderate and high seastates, second order predictions underestimate the surge wave drift coefficients for all compared diagonals of the QTFs. The discrepancies between predictions and empirical coefficients are not small, especially at the lower frequency range (below around 0.10 Hz) where the potential flow wave drift forces tend to zero.

1. Introduction

Safe and cost-effective design of mooring systems for floating wind turbines require a correct prediction of wave drift loads. The related low frequency motions have a significant contribution to the extreme loads on the station keeping system. Newman's approximation ([1]), which relies on the use of mean wave drift coefficients only, is still widely applied by the industry to calculate the wave drift forces in irregular waves and, in fact, properly calibrated numerical models compare well with model test data even in severe seastates ([2]-[5]). However, full quadratic transfer functions (QTFs) of the low frequency excitation provide a more consistent and correct representation of the wave drift forces. There is less experience with the use of full QTFs calculated by second order potential flow codes for mooring analysis. A better understanding of its accuracy is needed and the related uncertainties and challenges must be properly addressed.

Although the current practice is to use potential flow methods to calculate wave-body interactions of large volume structures, there are limitations when calculating wave drift forces, especially in high seastates where the assumptions of perturbation theory may be violated. For column stabilized units, viscous wave drift loads become relevant if the wave amplitude is large enough compared to the columns' diameter ([6]-[9]). In fact, viscous effects may dominate the wave drift forces for long and large amplitude waves, since the potential flow counterpart tends to zero as the wavelength increases. Experimental evidence for the underestimation of wave drift forces by potential flow codes in steep seastates is provided, for example, in [9], [10], [11], [15] and [18]. For these reasons, it is of interest to

assess the applicability of existing potential flow numerical tools and identify their limitations. Systematic studies addressing this matter for floating wind turbines can be found in, e.g., [12], [13].

While the existing studies discuss viscous wave drift effects, or the low frequency (LF) motion responses, or some present attempts to identify mean wave drift coefficients and compare with predictions, the focus of this paper is on the full QTFs and on the limitations of the full second order potential flow solution. It presents a comparison between empirical and numerical quadratic transfer functions (QTFs) of the horizontal wave drift forces on the INO WINDMOOR floating wind turbine. The sub-structure is a semisubmersible with three columns connected by pontoons. The empirical QTFs are identified from model test data ([14]) obtained in an ocean basin using a second order technique known as cross bi-spectral analysis ([15],[16]). The procedure uses the calibrated incident wave elevation and the measured low frequency motion. The numerical QTFs are calculated by a radiation/diffraction potential flow code which solves the wave-structure first order and second order problems. Systematic comparisons between numerical and empirical QTFs allows identification of tendencies of empirical QTFs and limitations of the second order potential flow predictions.

The present study is limited to low frequency hydrodynamic loads from waves only, i.e. without current. For small seastates, the results indicate that the second order potential flow predictions of the surge QTFs agree quite well with the wave drift coefficients identified empirically from the model test data. This is an indication that second order potential flow theory predicts well the wave exciting QTFs for small seastates. For moderate and high seastates, second order predictions underestimate the surge wave drift coefficients for all compared diagonals of the QTFs. The discrepancies between predictions and empirical coefficients are not small, especially at the lower frequency range (below around 0.10 Hz) where the potential flow wave drift forces tend to zero.

The results will be useful to support the development of semi-empirical methods to correct the potential flow wave drift forces in moderate and high sea-states and to validate them.

2. Model tests

Model tests were performed in March 2020 in the Ocean Basin at SINTEF Ocean with the model of the INO WINDMOOR semi floating wind turbine. A Froude scaling of 1:40 was used for the tests with a full-scale water depth of 150 m. More detailed information about the tests can be found in [14].

The tests were performed to study 1) the low frequency (LF) response, 2) the coupling between the aerodynamic and hydrodynamic loads, and 3) the experimental uncertainty. Tests with waves only, wave and current, and wave and wind were performed. For the tests with wind the wind turbine rotor and tower loads were applied by use of the Real-Time Hybrid Model test method. A wide range of sea-states were used with pink-noise spectrum, small sea-states, and more severe sea-states and waves from 0 and 90 degrees (see Figure 2 for wave propagation definition). A JONSWAP wave spectrum was used for the irregular sea-states. The work presented here-in is focusing on objective 1 where only a selection of wave-only tests is used, see Table 2. Some seastates were repeated for several different realizations (different seeds) to reduce the sample variability of the identified QTFs. Hs and Tp stand for the sea state significant wave height and wave peak period, while γ represents the peak enhancement factor.

The model of the INO WINDMOOR is represented in Figure 1. The main dimensions and mass properties of the model are given in Table 1. The model was held in place during the tests by use of a simplified horizontal mooring system to remove any complexity due to mooring non-linearity and damping. The model was instrumented to measure the platform motions in 6 degrees of freedom, the relative wave elevation at 6 locations and the mooring line tensions at fairlead.

3. Procedure to identify empirical QTFs

3.1. Method

A method is applied to identify wave drift force coefficients for the semi from model test data. The data analysis technique is known as "cross-bi-spectral analysis" and it estimates characteristics of second-order responses (quadratic transfer functions – QTFs). The identified drift coefficients include mainly

the quadratic contents of the experimental signals, but they may also include higher-order contributions. While a brief explanation is given in the following paragraphs, details of the method can be found in [15] and [16].

The procedure follows two major steps. First, identify the second order wave exciting force (or moment) signal from the measured low frequency (LF) motion response. One assumes a linear mass-damper-spring system represents the LF motion. The system natural frequency, mass and linear spring constants are known. Decay tests provide information for initial assumption of system damping, which is adjusted through an iterative process. The second order excitation force is the only unknown to be determined.

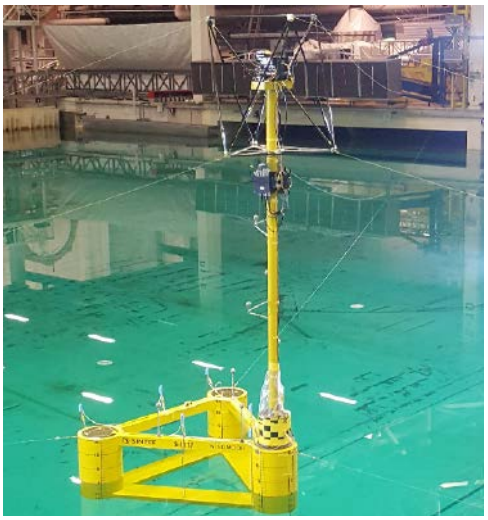

Figure 1: INO WINDMOOR scaled model.

Table 1: INO WINDMOOR main properties.

Parameter	Unit	Value
Column diameter	[m]	15.0
Column height	[m]	31.0
Pontoon width	[m]	10.0
Pontoon height	[m]	4.0
Centre-centre distance	[m]	61.0
Draft	[m]	15.5
Displacement	[t]	14124
Vert. centre of gravity (VCG)**	[m]	19.4
Roll radius of gyration (Rxx)	[m]	43.6
Pitch radius of gyration (Ryy)	[m]	44.0
Yaw radius of gyration (Rzz)	[m]	29.9

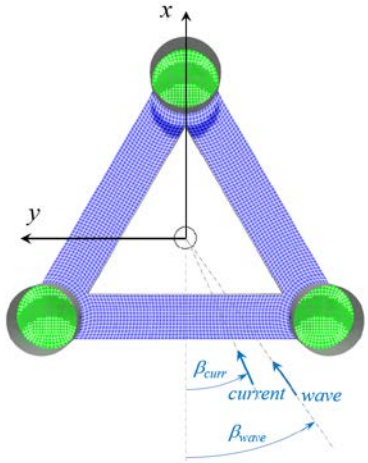

Figure 2: Coordinate system and convention for wave direction (the *z*-axis points upwards).

Table 2: List of tests and related seastate parameters.

Number of seeds	Hs (m)	Tp (s)	γ
6	2.0	7.0	1.06
5	3.7	7.0	4.90
6	6.2	9.0	4.90
2	6.2	12.0	1.23
6	11.0	12.0	4.90
1	15.0	14.0	4.90

Second, use the undisturbed incident wave elevation and the estimated second order force, together with cross bi-spectral analysis, to identify the difference frequency wave exciting QTF matrix:

$$H^{(2)}(f_m, f_n) = \frac{S_{\zeta\zeta g}(f_m, f_n)}{S_{\zeta\zeta}(f_m) S_{\zeta\zeta}(f_n)}$$

where $H^{(2)}(f_m, f_n)$ is the wave drift force coefficient corresponding to the wave frequency pair (f_m, f_n), $S_{\zeta\zeta}(f_m)$ represents the wave spectrum and $S_{\zeta\zeta g}(f_m, f_n)$ is the cross bi-spectrum of the second order excitation with respect to the incident wave elevation.

Although the principle is simple, achieving stable numerical solution for the QTF is not simple in practice. The main difficulty is related to the statistical averaging of the cross bi-spectrum $S_{\zeta\zeta g}$. Stansberg [15] discusses further this aspect, where a particular noise reduction method is introduced based on image processing principles.
The method described in the previous paragraphs is applied to identify the QTFs of wave drift forces and linearized LF damping of the INO WINDMOOR semi.

3.2. Example

This Section presents an example of the results from the cross bi-spectral analysis and the procedure to validate the identified QTF. The example corresponds to a test case where Hs is 3.74 m and Tp is 7 s (test 4220). The test duration was 3.3 hours, full scale, and the initial 20 minutes were removed before the time signals were used for the cross bi-spectral analysis. The same procedure was used for all irregular wave analyses.

Figure 3 shows the estimated surge QTF of the difference-frequency wave exciting forces. The bi-frequency plane axes are in Hz and the colors represent the wave drift coefficients magnitude in kN/m^2. Dashed white lines follow diagonals with constant difference-frequency of 0.011 Hz, which corresponds to the surge natural frequency.

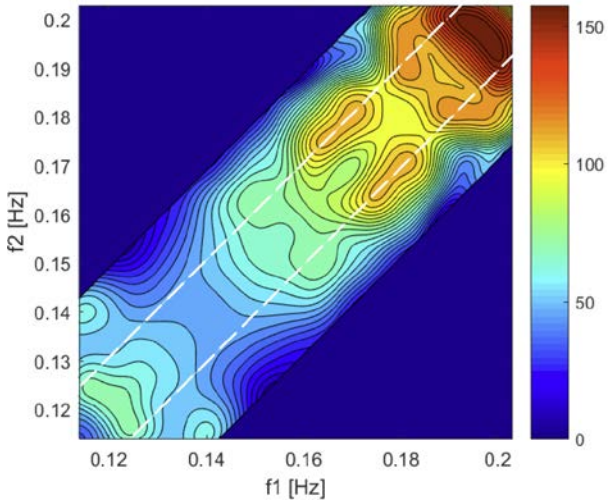

Figure 3: Empirical surge QTF modulus identified from test 4220 (Hs=3.74m, Tp= 7 s, heading = 0). Coloured scale in kN/m^2.

The quality of the identified QTF is assessed by comparing the measured low frequency motion (measured signals low pass filtered at 0.03 Hz) with the low frequency motion calculated using wave exciting forces reconstructed from the identified QTF. The comparison is done in terms of time histories and low frequency spectra. An example for surge and the same test case is presented in Figure 4 and Figure 5. The agreement between measured and reconstructed signals is good, which validates the QTF empirical estimation.

Low frequency (LF) bound waves and parasitic waves are a challenge with tests in shallow water [19] and they need to be considered in the QTF identification based on model tests. However, these LF components are small in deep water, as used in the present study, and their effects on the LF motions assumed negligible.

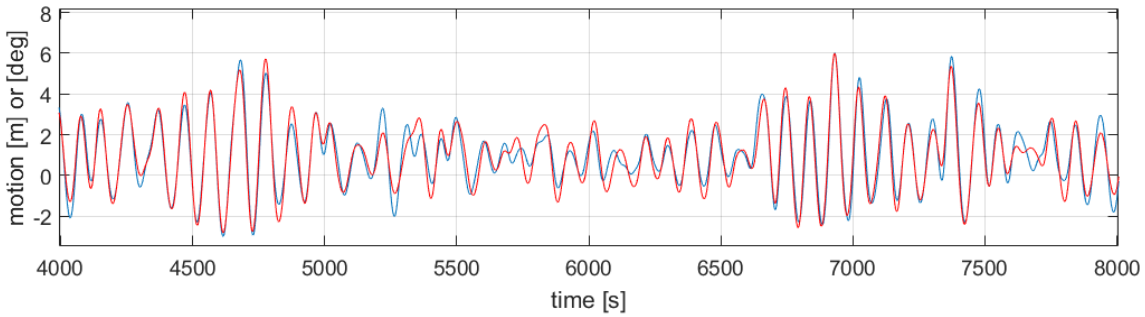

Figure 4: Comparison between measured slow drift surge motion (blue line) and reconstructed from the identified empirical QTF (red line). Results from test 4220 (Hs=3.74m, Tp= 7 s, head. = 0).

4. Numerical model

The potential flow calculations are performed with Hydrostar v8.10 [20], [21]. The code is based on the boundary element method and it solves the wave-structure first order and second order radiation/diffraction problems.

The first order solution gives the motion response amplitude operators (RAOs), among other first order results. Mean wave drift force coefficients are calculated from the first order results. The second order solution at the difference-frequency for pairs of harmonic waves gives the QTFs of wave drift forces. The numerical solution is established by discretizing the mean hull wetted surface into a finite number of flat panels. The wave drift coefficients are evaluated by the "middle field" method, which requires a control surface surrounding the hull and closed at the free surface. Expressions for the quadratic forces are evaluated on the control surface, instead of over the hull surface, with advantages in terms of accuracy for the estimation of the required fluid velocity terms.

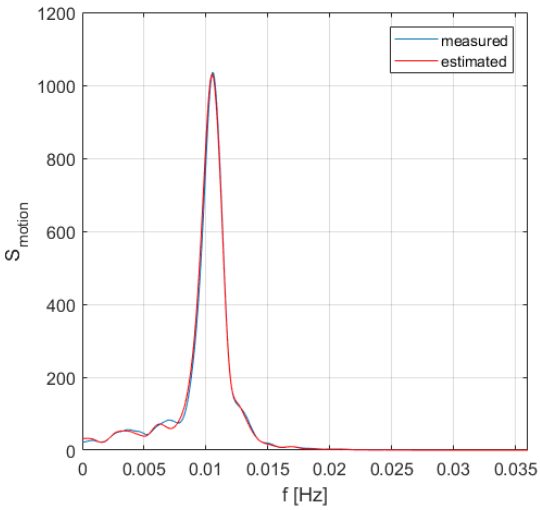

Figure 5: Comparison between experimental (blue) and reconstructed from the identified QTF (red) LF surge spectra. Results from test 4220 (Hs=3.74m, Tp= 7 s, head. = 0).

The free surface integral in the second order solution is neglected. The assumption is that the effects of this term are small for small difference frequencies typical of the natural frequencies for the horizontal motions of moored floating structures. The free surface integral term is of order of the difference frequency squared, $O[(\Delta\omega)^2]$, or higher [19]. Effects of the free surface integral are expected to be more important for the heave, roll and pitch LF motions since the natural frequencies are higher.

The potential flow calculations are carried out for the relevant range of wave frequencies and difference frequencies. Table 3 presents the number of first order panels used to represent the hull surface and the control surface. Altogether the mesh accounts for 17176 panels. Figure 6 shows the hull mesh and the control surface mesh. A convergence study on the hull mesh was performed in terms of first order responses and mean wave drift coefficients.

Additional stiffness coefficients in surge, sway and yaw represent the mooring system effects. Finally, additional damping coefficients are applied in all modes of motion to represent linearized viscous damping effects and in this way limit the RAOs resonant peaks to realistic values. This is important since the QTFs depend on the wave frequency motions, therefore the level of damping will affect the QTF prediction, especially around the motions resonance frequencies. Table 4 presents the additional restoring and relative damping coefficients defined as the actual damping coefficient normalized by the critical damping. The additional damping coefficients were tuned to achieve a good match between predicted and measured motion transfer function resonance peaks for moderate seastates.

Table 3: Number of low order panels of the numerical model.

Surface	Number of panels
Vessel hull surface	11212
Interior free surface	0
Control surface	5964
Total	17176

Table 4: Mooring restoring coeffs. and additional damping coeffs. applied for the radiation/diffraction analysis.

	Rest. coeff. [N/m] or [Nm]	Damp. coeff. [Ns/m] or [Nms]	Relative damping [-]
Surge	8.98E+04	1.42E+05	0.05
Sway	8.98E+04	1.42E+05	0.05
Heave	0	1.50E+06	0.05
Roll	0	6.96E+08	0.05
Pitch	0	6.95E+08	0.05
Yaw	1.22E+08	1.61E+08	0.03

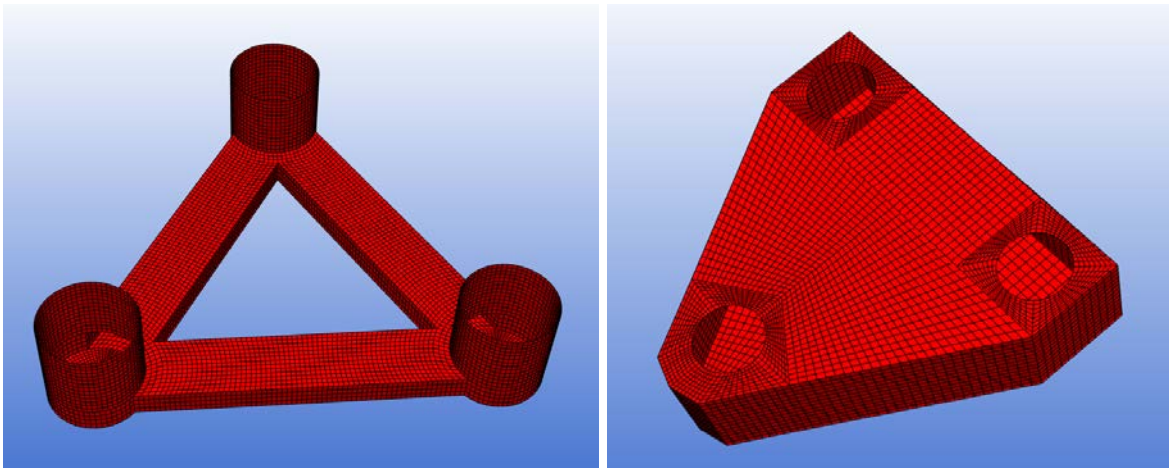

Figure 6: INO WINDMOOR body mesh (left) and control surface mesh for middle field calculations (right).

5. Results

This Section compares empirical QTFs of the surge wave drift forces identified from the model test data with numerical QTFs calculated by the second order potential flow code. The QTFs are compared in terms of diagonals with constant difference-frequency (f2-f1 in the plots). The related figures, presented in the following pages, include plots for 4 difference frequencies (df=f2–f1), where the first plot always correspond to a df = 0, therefore it represents the mean wave drift coefficients. The remaining difference frequencies are equally spaced and the largest one goes beyond the df corresponding to the natural frequency, which in this case is f_n = 0.011 Hz. The contribution from wave drift forces to the platform mean motion offset in irregular waves depends on the coefficients corresponding to df = 0 (mean wave drift coefficients). On the other hand, the slowly varying oscillations induced by the wave drift forces depend on a narrow difference frequency band around the motion natural frequency. The reason is that the low frequency motion is tuned around the natural frequency where it shows a dynamic amplification. The width of the relevant difference frequency band increases with the system damping, therefore it increases with seastate severity.

The referred figures include plots with the real part, the imaginary part and the absolute value. Each plot includes three lines corresponding to the experimental QTF (or empirical QTF), numerical QTF and combined QTF. Combined means that the empirical curves are merged with the numerical ones for low and high wave frequencies and for large difference frequencies. The reason to combine is that the empirical QTF does not include information outside the tested wave frequency range and outside the measured LF motion signal frequency content. The combined QTFs will be used for future simulation of the floater low frequency motions.

The following analysis is separated into "Small seastates" and " Moderate and high seastates". One should note that the empirical coefficients have some inherent uncertainty related to the finite duration of the time series. The effective length of the time records is three hours, which results in around 115 low frequency cycles for surge. For this reason, tests for several of the seastates were repeated with different seeds. The related empirical QTFs represent averaging of the QTFs estimated for each of the seeds. These estimates are considered more reliable, meaning with lower sample variability. Table 2 presents the seastates which have several realizations.

Furthermore, the empirical estimates are more reliable for the difference-frequency range around the natural frequency and for the wave frequency range where the seastate has energy. The reason is that the information in the low frequency motion signal and wave elevation signal is within these frequency ranges. For the same reason, zero difference-frequency estimates are in general less reliable, as well as estimates for low and high wave frequency ranges.

5.1. Small seastates

Figure 7 presents the surge QTF for a small seastate with Hs = 2.0 m and Tp = 7 s. One observes a good correlation between the numerical predictions and the empirical coefficients, both for the real and the imaginary parts and for the different diagonals of the QTF. The observation is not valid for the for higher frequencies around 0.25 Hz where the numerical QTF modulus is larger than the empirical one. It is not obvious if the discrepancy represents overestimation by the numerical predictions, or uncertainty of the empirical results because this frequency range is at the tail of the wave spectrum and the energy is small. In any case, it is possible to say that the general agreement is quite good, which indicates that the second order potential flow theory correctly represents the physics of the low frequency excitation. This conclusion is valid for the horizontal force, surge in this case, for small amplitude waves and conditions without current.

The results also show that the surge wave drift forces are dominated by the real part of the QTF, while the relative importance of the imaginary component tends to increase with the difference frequency. This behavior is captured by both the numerical results and the empirical estimation.

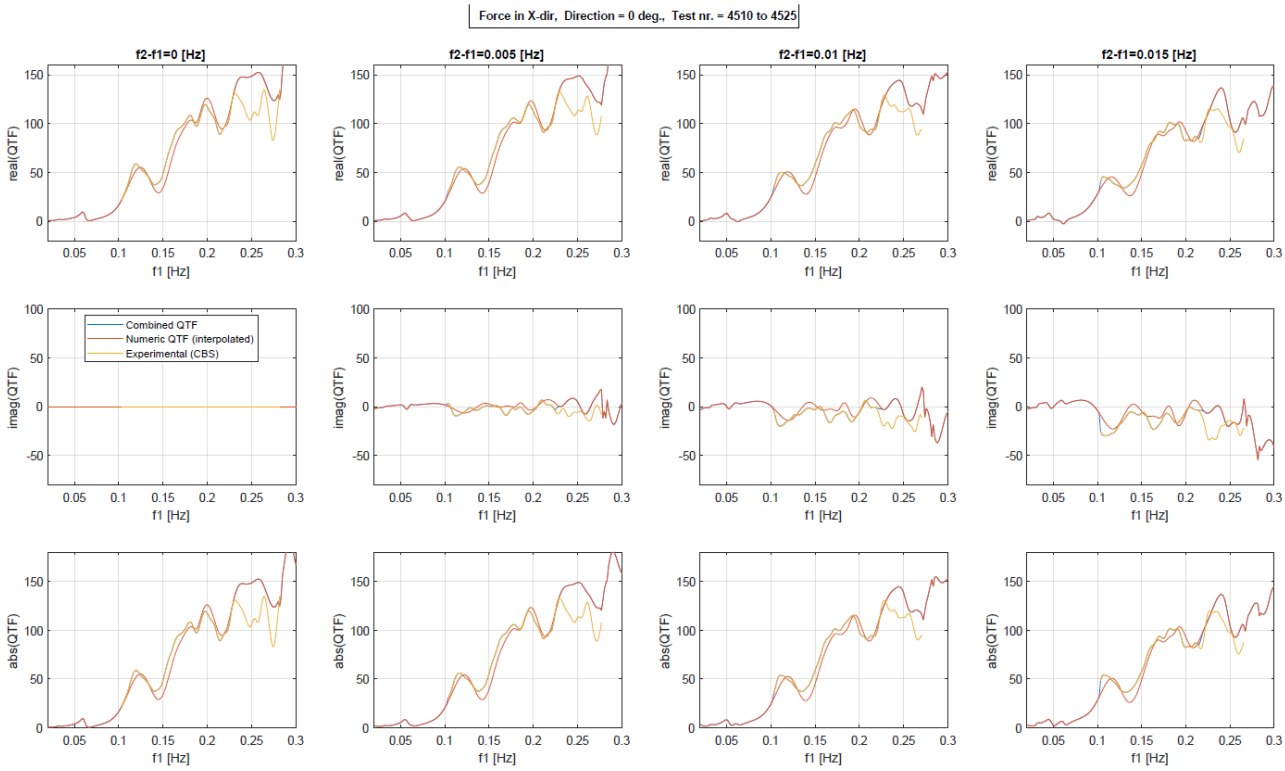

Figure 7: Surge QTF. Tests 4050 to 4525 with Hs = 2.0 m, Tp = 7 s, Heading = 0 deg.

5.2. Moderate and high seastates

The focus is again on the surge QTF for 0 degrees wave heading and we separate the "Moderate and severe seastates" into:

a) Two moderate sea-states which provide QTF information at the intermediate frequency range – between 0.10 and 0.15 Hz – namely tests 4230 to 4244 and tests 4290 to 4292

b) Two severe sea-states which provide QTF information at the low frequency range only – below around 0.12 Hz – namely tests 4662 to 4677 and test 4560.

Starting with case a), there is an underestimation of the empirical QTF by the potential flow results (Figure 8 and Figure 9) for the frequency range between 0.10 and 0.12 Hz. The fact that the empirical QTF is identified over a relatively narrow wave frequency band is related to the fact that the wave spectrum is also narrow banded and therefore there is not much wave energy outside this band.

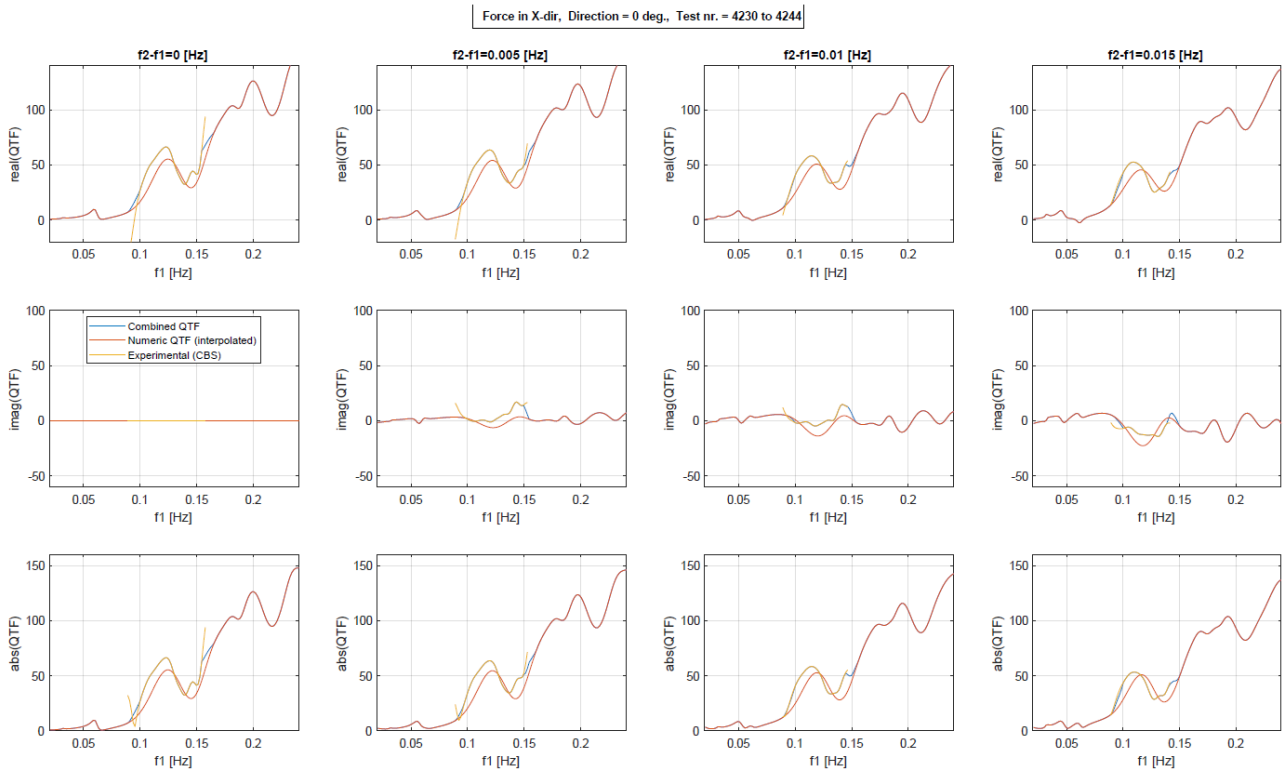

Figure 8: Surge QTF. Tests 4230 to 4244 with Hs = 6.2 m, Tp = 9.0 s, Heading = 0 deg.

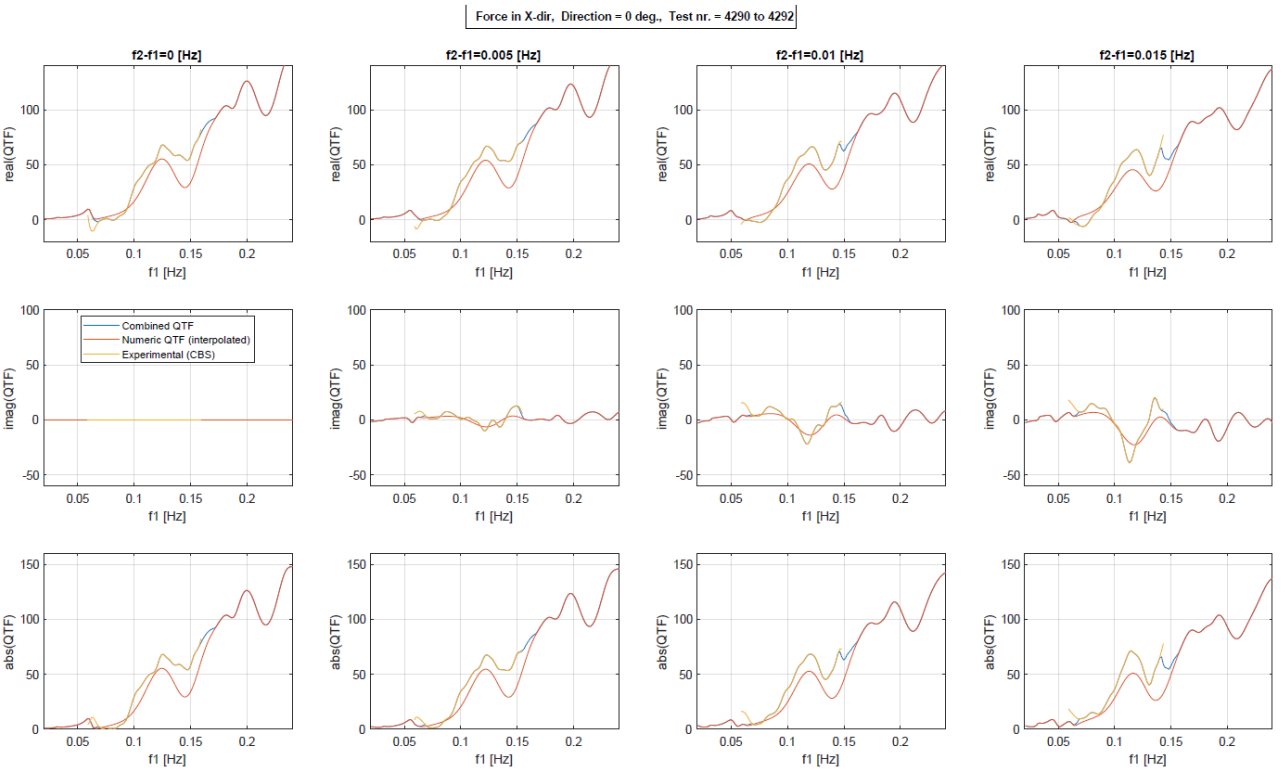

Figure 9: Surge QTF. Tests 4290 and 4292 with Hs = 6.2 m, Tp = 12.0 s, Heading = 0 deg.

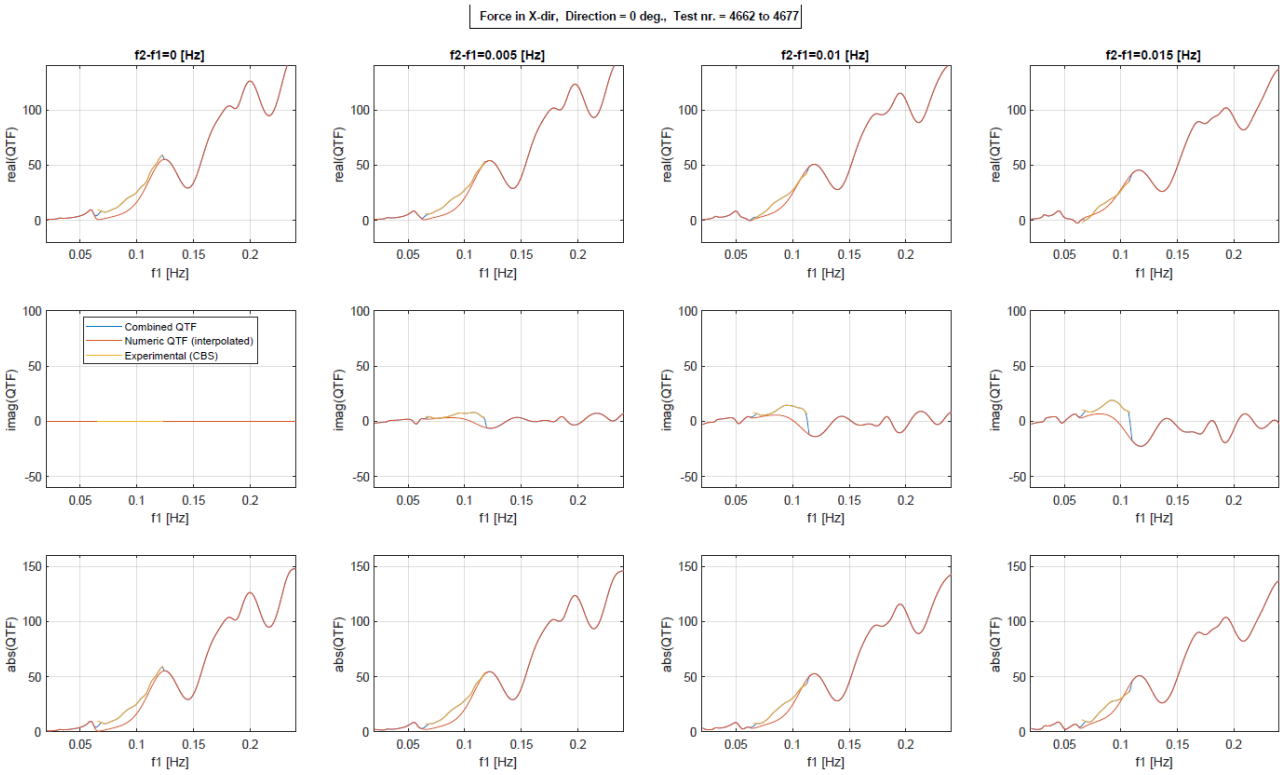

Figure 10: Surge QTF. Tests 4662 to 4677 with Hs = 11.0 m, Tp = 12.0 s, Heading = 0 deg.

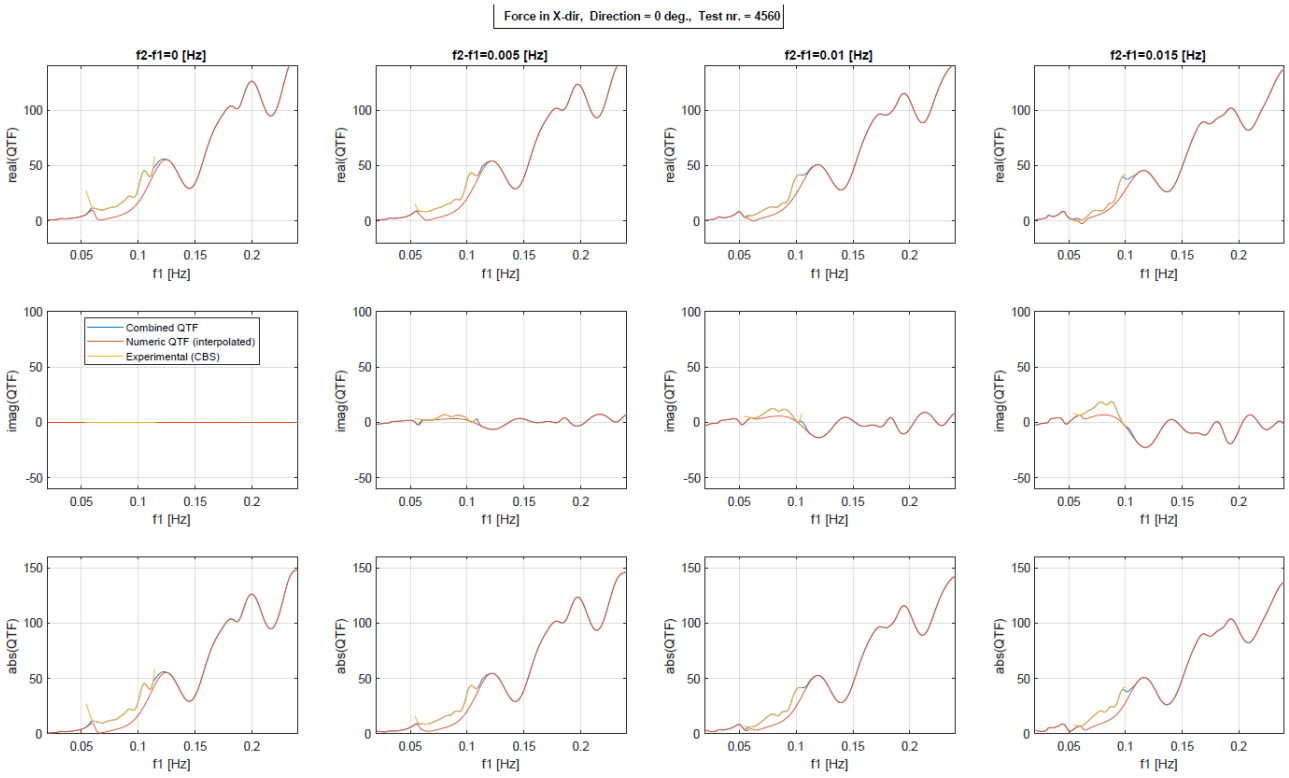

Figure 11: Surge QTF. Tests 4565 with Hs = 15.0 m, Tp = 14.0 s, Heading = 0 deg.

Regarding the seastates with longer wave peak periods, the plots show, again, an underestimation of the empirical QTF by the potential flow results (Figure 10 and Figure 11). The underestimation may not appear to be significant at first sight. However, one should note that the related seastates have peak

periods of 0.07 and 0.08 Hz, therefore the empirical coefficients show the wave drift forces are around double the numerical predictions for the relevant wave frequency range.
The underestimation at the low frequency range is believed to be related to viscous wave drift effects which are neglected by the potential flow code. As observed before, there is also underestimation for the intermediate frequency range (0.12 to 0.15 Hz). The relative importance of viscous wave drift is probably much smaller for the intermediate frequencies, therefore the differences may also be related to higher than second order potential flow effects.

6. Conclusions

The study applies a second order signal analysis method to model test data with waves only (no wind nor current) to identify empirical quadratic transfer functions (QTFs) of the surge wave drift forces for a semi-submersible FWT. Systematic comparisons between numerical and empirical QTFs allows identification of tendencies of empirical QTFs and limitations of the second order potential flow predictions.

For small seastates, the available results indicate that the second order potential flow predictions of the surge QTFs agree quite well with the wave drift coefficients identified empirically from the model test data. This is an indication that second order potential flow theory predicts well the wave exciting QTFs for small seastates with no current.

For moderate and high seastates, second order predictions underestimate the surge wave drift coefficients for all compared diagonals of the QTFs. The discrepancies between predictions and empirical coefficients are not small, especially at the lower frequency range (below around 0.10 Hz) where the potential flow wave drift forces tend to zero. For the seastates with longer wave periods, the experimental wave drift forces are around double those predicted by the potential flow code. The discrepancies at the low frequency range are believed to be related to viscous wave drift loads which are neglected by potential flow codes. For the intermediate frequency range, viscous wave drift probably plays a smaller role, therefore the differences may also be related to higher than second order potential flow effects.

The systematic identification of the second order potential flow solution limitations presented herein can be used to develop and test semi-empirical methods to correct the potential flow wave drift forces in moderate and high sea-states.

Acknowledgments

The research leading to these results has received funding from the Research Council of Norway through the ENERGIX programme (grant 294573) and industry partners Equinor, MacGregor, Inocean, APL Norway and RWE Renewables.

The authors are grateful for the permission to use the INO WINDMOOR semisubmersible, which is jointly designed by Inocean and Equinor.

References

[1] Newman N., 1974. Second-order, slowly-varying forces on vessels in irregular waves. Proc. Symp. on the Dyn. of Marine Vehicles and Struct. in Waves, London, UK, 182-186.

[2] Aksnes, V., Berthelsen, P.A., Fonseca, N., and Reinholdtsen, S.-A., 2015. On the need for calibration of numerical models of large floating units against experimental data. Proc. of the Int. Offshore and Polar Eng. Conference, Kona, Hawaii, USA, paper ISOPE2015-TPC0463.

[3] Ommani, B., Fonseca, N. and Stansberg, C.T., 2017. Simulation of low frequency motions in severe seastates accounting for wave-current interaction effects. Proc. of the ASME 2017 36th Int. Conf. on Ocean, Offshore and Arctic Eng., June 25-30, 2017, Trondheim, Norway, paper OMAE2017-62550

[4] Fonseca, N., Ommani, B., Stansberg, C.T., Bøckmann, A., Birknes-Berg, J., Nestegård, A., de Hauteclocque, G., Baarholm, R., 2017. Wave Forces and Low Frequency Drift Motions in Extreme Seas: Benchmark Studies. Proceedings of the Offshore Technology Conference,

paper OTC-27803-MS, 1-4 May 2017, Houston, TX, USA
[5] Fonseca, N., Stansberg, C.T., 2018. Calibration of a time domain numerical hydrodynamic model for mooring analysis of a semi-submersible. Proc. of the ASME 2018 37th Int. Conf. on Ocean, Offshore and Arctic Eng., June 17-22, 2018, Madrid, Spain, paper OMAE2018-78753.
[6] Dev, A.K. and Pinkster, J.A., 1994, "Experimental evaluation of the viscous contribution to mean drift forces on vertical cylinders. Proceedings 7th International Conference on the Behaviour of Offshore Structures (BOSS'94), MIT, Editor C. Chyssostomidis, Elsevier, **2**, pp. 855 - 875.
[7] Dev, A.K. and Pinkster, J.A., 1995. Viscous mean drift forces on moored semi-submersibles. Proc., 5th Int. Offshore and Polar Eng. Conference, The Hague, The Netherlands, June 11-16.
[8] Berthelsen, P.A., Baarholm, R., Pakozdi, C., Stansberg, C.T., Hassan, A., Downie, M. and Incecik, A., 2009. Viscous drift forces and responses on a semisubmersible platform in high waves. Proceedings Int. Conference on Offshore Mechanics and Arctic Engineering, Honolulu, Hawaii, 31st May – 5th June, paper OMAE2009-79483.
[9] Berthelsen, P.A., Bachynski, E., Karimirad, M., and Thys, M., 2016. Real-Time hybrid model tests of a braceless semi-submersible wind turbine. Part III: Calibration of a numerical model. Proceedings Int. Conference on Offshore Mechanics and Arctic Engineering, Busan, Korea, 19th-24th June, paper OMAE2016-54640.
[10] Robertson, A. N., et al., 2017. OC5 project phase II: Validation of global loads of the DeepCwind floating semisubmersible wind turbine". Energy Procedia, 137, pp. 38–57.
[11] Kvittem, M.I., Berthelsen, P.A., Eliassen, L., and Thys, M., 2018, Calibration of hydrodynamic coefficients for a semi-submersible 10 mw wind turbine. Proc. Int. Conference on Offshore Mechanics and Arctic Engineering, Madrid, Spain, 17th-22th June, paper OMAE2018-77826.
[12] Simos A. N., Ruggeri F., Watai R. A., Souto-Iglesias A., and Lopez-Pavon, C. 2018. Slow-drift of a floating wind turbine: An assessment of frequency-domain methods based on model tests. Renewable Energy, 116, pp. 133-154.
[13] Robertson, A.N., et al., 2020. OC6 Phase I: Investigating the under-prediction of lowfrequency hydrodynamic loads and responses of a floating wind turbine. J. Phys.: Conf. Ser. 1618 (TORQUE 2020).
[14] Thys, M., Souza, C.E.S., Fonseca, N., Berthelsen, P.A., Engebretsen, E., and Haslum, H., 2021. Experimental Investigation of a new 12MW semi-submersible floating wind turbine. Proceedings Int. Conference on Offshore Mechanics and Arctic Engineering, 21-30 June, OMAE2021- 62980 (to be published).
[15] Stansberg, C.T., 1997. Linear and nonlinear system identification in model testing. International Conference on Nonlinear Aspects of Physical Model Tests, OTRC, Texas A&M University, College Station, Texas, 2-3 May 1997.
[16] Stansberg, C.T. 2001. Data Interpretation and System Identification in Hydrodynamic Model Testing. Proc. of 11th Int. Offshore and Polar Eng. Conf., ISOPE, Stavanger, Norway.
[17] Fonseca, N. and Stansberg, C.T., 2017, "Wave drift forces and low frequency damping on the Exwave Semi-submersible", Proc. of the ASME 2017 36th Int. Conf. on Ocean, Offshore and Arctic Eng., June 25-30, 2017, Trondheim, Norway, paper OMAE2017-62540.
[18] Fonseca, N., Stansberg, C.T., Larsen, K., Bjørkly, R., Vigesdal, T. and Dalane, O., 2021. Low frequency wave loads and damping of four MODUs in severe seastates with current. *Journal* of Offshore Mechanics and Arctic Engineering, 143 (1).
[19] Fonseca, N., Tahchiev, G., Fouques, S., Stansberg, C.T., Rodrigues, J.M., 2020. Model Tests and Numerical Prediction of the Low Frequency Motions of a Moored Ship in Shallow Water with a Wave Splitting Method. Proc. of the ASME 2020 39th Int. Conf. on Ocean, Offshore and Arctic Eng., June 21-30, 2020, Virtual, paper OMAE2020-18806.
[20] Bureau Veritas, 2019. Hydrostar for experts user manual. January 2019.
[21] Chen, X.B, 2007. Middle-field formulation for the computation of wave-drift loads. Journal of Engineering Mathematics, 59(1): 61-82.